The prionlike domain of FUS is multiphosphorylated following DNA damage without altering nuclear localization

Shannon N. Rhoads[a], Zachary T. Monahan[a], Debra S. Yee[a], Andrew Y. Leung[a], Cameron G. Newcombe[a], Robert N. O'Meally[b], Robert N. Cole[b], and Frank P. Shewmaker[a,*]
[a]Department of Pharmacology and Molecular Therapeutics, Uniformed Services University, Bethesda, MD 20814; [b]Department of Biological Chemistry, Johns Hopkins Mass Spectrometry and Proteomic Facility, Johns Hopkins University, Baltimore, MD 21205

ABSTRACT **FUS (fused in sarcoma) is an abundant, predominantly nuclear protein involved in RNA processing. Under various conditions, FUS functionally associates with RNA and other macromolecules to form distinct, reversible phase-separated liquid structures. Persistence of the phase-separated state and increased cytoplasmic localization are both hypothesized to predispose FUS to irreversible aggregation, which is a pathological hallmark of subtypes of amyotrophic lateral sclerosis and frontotemporal dementia. We previously showed that phosphorylation of FUS's prionlike domain suppressed phase separation and toxic aggregation, proportionally to the number of added phosphates. However, phosphorylation of FUS's prionlike domain was previously reported to promote its cytoplasmic localization, potentially favoring pathological behavior. Here we used mass spectrometry and human cell models to further identify phosphorylation sites within FUS's prionlike domain, specifically following DNA-damaging stress. In total, 28 putative sites have been identified, about half of which are DNA-dependent protein kinase (DNA-PK) consensus sites. Custom antibodies were developed to confirm the phosphorylation of two of these sites (Ser-26 and Ser-30). Both sites were usually phosphorylated in a subpopulation of cellular FUS following a variety of DNA-damaging stresses but not necessarily equally or simultaneously. Importantly, we found DNA-PK–dependent multiphosphorylation of FUS's prionlike domain does not cause cytoplasmic localization.**

Monitoring Editor
Orna Cohen-Fix
National Institutes of Health

Received: Dec 21, 2017
Revised: May 18, 2018
Accepted: Jun 5, 2018

INTRODUCTION

FUS (fused in sarcoma) is a ubiquitously expressed DNA/RNA-binding protein implicated in diverse functions, including transcription (Tan *et al.*, 2012; Yang *et al.*, 2014b), RNA splicing (Ishigaki *et al.*, 2012; Lagier-Tourenne *et al.*, 2012; Rogelj *et al.*, 2012), mRNA transport (Fujii and Takumi, 2005; Fujii *et al.*, 2005), and the DNA damage response (Mastrocola *et al.*, 2013; Wang *et al.*, 2013). Mislocalization of FUS into neuronal cytoplasmic inclusions is implicated in subtypes of amyotrophic lateral sclerosis (ALS) (Kwiatkowski *et al.*, 2009; Vance *et al.*, 2009) and frontotemporal dementia (FTD) (Neumann *et al.*, 2009).

The FUS protein is 526 amino acids, containing a C-terminal nuclear localization signal, three arginine/glycine-rich domains, a zinc finger domain, an RNA recognition motif, and a long N-terminal prionlike domain (PrLD; ~160 amino acids). The PrLD has low sequence complexity, primarily consisting of glycine, glutamine, serine, threonine, and tyrosine. This composition, with its paucity of charged and aliphatic amino acids, is similar to the domains in yeast proteins that enable prion proliferation through the formation of self-propagating amyloid fibers. Because PrLDs are found in many

This article was published online ahead of print in MBoC in Press (http://www.molbiolcell.org/cgi/doi/10.1091/mbc.E17-12-0735) on June 13, 2018.

*Address correspondence to: Frank P. Shewmaker (frank.shewmaker@usuhs.edu).

Abbreviations used: ALS, amyotrophic lateral sclerosis; ATM, ataxia-telangiectasia mutated; DNA-PK, DNA protein kinase; FTD, frontotemporal dementia; FUS, fused in sarcoma; IR, ionizing radiation; LLPS, liquid–liquid phase separation; PrLD, prionlike domain; PTM, posttranslational modifications; siRNA, small interfering RNA.

proteins that form pathological inclusions in neurodegenerative diseases, it is speculated they contribute to aggregation processes in neurons. In vitro, the PrLD of FUS forms archetypical amyloid structure (Murray *et al.*, 2017) and can undergo liquid–liquid phase separation (LLPS) (Burke *et al.*, 2015), a phenomenon in which macromolecules form dense dynamic assemblies distinct from the bulk solvent environment (Burke *et al.*, 2015; Murakami *et al.*, 2015; Patel *et al.*, 2015; Monahan *et al.*, 2017; Murray *et al.*, 2017). Recombinant FUS will phase separate in vitro to form dynamic liquid droplets, which over time can evolve into irreversible solid aggregates (Murakami *et al.*, 2015). It is hypothesized that aberrant protein interactions within condensed phase-separated assemblies may facilitate formation of similar intractable solid aggregates in diseased neurons (Patel *et al.*, 2015).

In healthy neurons, and in cell lines and primary culture under typical growth conditions, FUS appears to be mostly nuclear (Hoell *et al.*, 2011; Dormann *et al.*, 2012; Yasuda *et al.*, 2013; Deng *et al.*, 2014; Schwartz *et al.*, 2014). However, in diseased neurons, FUS accumulates into cytoplasmic inclusions (Vance *et al.*, 2009). Cellular pathology follows along neuroanatomical pathways, suggesting "prionlike" spread of protein aggregates (Armstrong, 2017). Cytoplasmic FUS inclusions are proposed to have an emergent gain-of-function toxicity (Sharma *et al.*, 2016; Devoy *et al.*, 2017) possibly resulting from altered cytoplasmic RNA binding (Hoell *et al.*, 2011; Daigle *et al.*, 2013). However, neuronal degeneration may also result from loss of FUS function due to nuclear depletion (Sun *et al.*, 2015). In either scenario, preventing FUS cytoplasmic aggregation and accumulation could provide therapeutic benefits for FUS-linked disease.

Several studies found posttranslational modifications (PTMs), including phosphorylation (Gardiner *et al.*, 2008; Kino *et al.*, 2011; Deng *et al.*, 2014; Darovic *et al.*, 2015) and arginine methylation (Rappsilber *et al.*, 2003; Tradewell *et al.*, 2011; Dormann *et al.*, 2012; Sama *et al.*, 2013; Scaramuzzino *et al.*, 2013), to be significant to FUS activity or localization in cell models. Two related kinases, DNA-PK and ATM (ataxia-telangiectasia mutated), have been linked to FUS activity. Both kinases are involved in the DNA damage response pathway (Blackford and Jackson, 2017) and were reported to specifically cause phosphorylation of the FUS PrLD following DNA double-strand breaks (Gardiner *et al.*, 2008; Deng *et al.*, 2014). In vitro, DNA-PK treatment of recombinant FUS results in phosphorylation at multiple sites in the PrLD, including DNA-PK/ATM consensus sites (serine or threonine followed by a glutamine; S/TQ) (Han *et al.*, 2012; Monahan *et al.*, 2017; Murray *et al.*, 2017). Previously, we explored the potential effects of phosphorylating these sites (Monahan *et al.*, 2017). We discovered that introduction of multiple phosphomimetic substitutions in FUS's PrLD dramatically reduced LLPS and formation of solid toxic aggregates, suggesting a therapeutic mechanism for inhibiting pathological aggregation.

Though several studies have focused on the effects of FUS phosphorylation on aggregation or LLPS, only a single phosphorylation site in the FUS PrLD has been confirmed in human cells (Gardiner *et al.*, 2008; Deng *et al.*, 2014) despite identification of numerous putative sites (Monahan *et al.*, 2017). Moreover, the conditions that cause phosphorylation and the extent of their effects on FUS are relatively unstudied. Here we continued exploration of candidate phosphorylation sites in FUS's PrLD using mass spectrometry and human cell lines. On the basis of our data, we generated phospho-specific antibodies to two positions in the FUS PrLD. With these novel antibodies, we monitored FUS phosphorylation and localization patterns following DNA damage. A consistent pattern of phosphorylation and localization was reproducibly observed in multiple cell lines.

RESULTS

The FUS prionlike domain is phosphorylated at numerous serines and threonines following calicheamicin treatment

Deng and coworkers found several pharmacological agents caused a characteristic increase in the apparent molecular weight of the FUS protein band in Western blots (Deng *et al.*, 2014): staurosporine (kinase inhibitor), calicheamicin (DNA damaging agent), and calyculin-A (phosphatase inhibitor). When they treated H4 neuroglioma cells with staurosporine, it yielded a high-molecular-weight FUS species that on phosphatase treatment returned to the untreated size, suggesting that the gel shift was due to phosphorylation. We reproduced their results showing an increase in FUS's apparent molecular weight in multiple human cell lines treated with staurosporine, calicheamicin, and calyculin-A (Figure 1A and Supplemental Figure S1A). Likewise, when we subjected immunoprecipitated FUS from calicheamicin and calyculin-A–treated cells to phosphatase before Western blotting, the FUS bands returned to their original, untreated position (Figure 1B). Additionally, we expressed FUS in H4 cells with various numbers of phosphomimetic substitutions (replacing S or T with E; see *Materials and Methods* for specific sites) to simulate varying amounts of phosphorylation in the PrLD. The mimetic FUS Western blot bands migrated at increasingly higher apparent molecular weights (Figure 1C) with the number of phosphomimetic substitutions correlated to the increase in band shift. A stepwise change became prominent above the unmodified FUS band with ~4 substitutions. The phosphomimetic with 12 substitutions (12E) migrated most similarly to FUS from staurosporine-, calicheamicin-, or calyculin-A–treated cells. From this, we concluded the large increase in apparent molecular weight in Western blots was consistent with multiple phosphorylation of FUS's PrLD.

Our previous work with recombinant DNA-PK indicated that all 12 S/TQ DNA-PK consensus motifs in the PrLD could be phosphorylated in vitro (Monahan *et al.*, 2017). We preliminarily mapped three of these sites using mass spectrometry analysis of immunoprecipitated FUS from HEK293T cells treated with calyculin-A: Ser-26, Ser-30, and Ser-61. Here, using refinements of our previous proteomic approach to identify PTMs, we focused our attention on the DNA-damaging agents calicheamicin and camptothecin, due to the previously implicated link between DNA damage and FUS phosphorylation. Numerous unambiguous S and T sites were identified (Supplemental Figure S2A). Several ion fragments appeared to contain two phosphates, albeit with less certainty (Supplemental Figure S2B). Site combinations within individual peptides were as follows: Ser-26/Ser-30, Ser-30/Ser-42, Thr-109/Ser-115, and Ser-115/Ser-117. In total, we found seven DNA-PK consensus sites in the PrLD to be phosphorylated following DNA damage with Ser-26 and Ser-30 being the most prominent across multiple experiments (Figure 1D). In general, the PrLD appears to be highly susceptible to multiphosphorylation in cells with as many as 28 candidate sites found by us and others (Figure 1D).

Ser-26 and -30 in the FUS prionlike domain are phosphorylated following DNA-damaging stress

Of the three drugs identified by Deng and colleagues to cause FUS phosphorylation, only calicheamicin has been established to directly cause DNA damage (Zein *et al.*, 1988; Deng *et al.*, 2014). Staurosporine is a promiscuous kinase inhibitor (Karaman *et al.*, 2008), and calyculin-A is an inhibitor of protein phosphatases 1/2A (Ishihara *et al.*, 1989). When HEK293T or H4 cells were treated with several DNA-damaging agents (e.g., etoposide, doxorubicin, camptothecin) or okadaic acid (phosphatase inhibitor similar to calyculin-A), we saw no characteristic band shift in FUS (Figure 2A). Phosphorylated

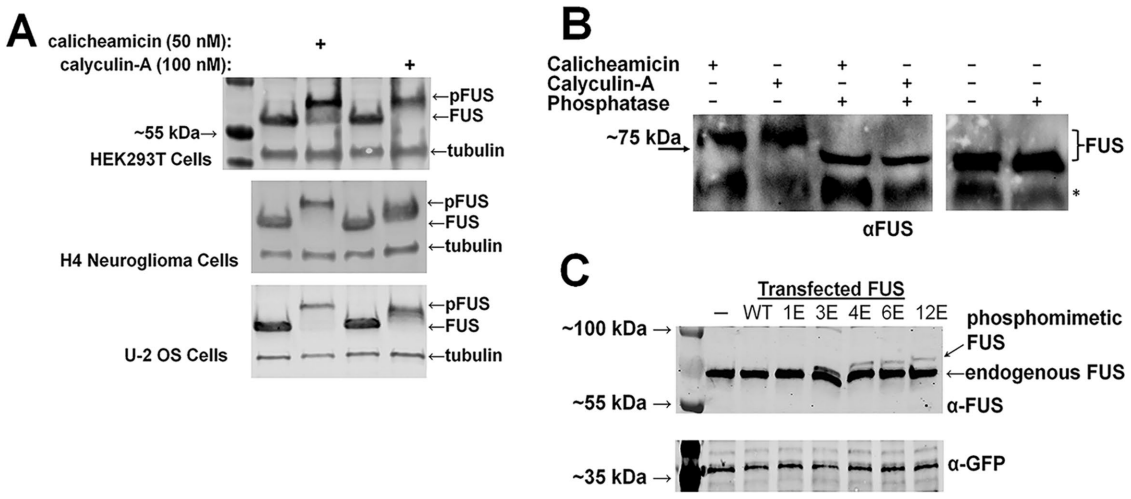

D

FUS (aa1-160)

MA**S**NDY**T**QQA **T**QSYGAYP**T**Q PGQGY**S**QQ**S**S QPYGQQ**S**YSG Y**S**QSTDTSGY GQS**S**YS**S**YGQ **S**QNTGYG**T**QS **T**PQGYG**ST**GG
YGS**S**QS**S**QSS YGQQ**SS**YPGY GQQPAPSS**TS** G**S**YGSS**S**QSS SYGQP**S**GSY **S**QQP**S**YGGQQ Q**S**YGQQQ**S**YN PPQGYGQQNQ

Phosphorylation sites	Identification Method	Source
T7, S26, S30, S37, **S42**, **S57**, S61, T71, S77, T78, S95, S96, T109, S110, S127, **S129**, S135, S148	IP & mass spec – calyculin A-treated HEK293 cells	**This study**; Monahan et al. 2017
T7, T11, T19, S26*, S30, S42*, S54, S61*, T68, S84*, S87, S112, S117, S131, S142	Mass spec – In vitro DNA-PK treated recombinant protein	Murray et al. 2017; *Han et al. 2012
T7, T11, T19, S26, S30, S42, S61, T68, S84, S87, S117, S131	NMR – In vitro DNA-PK treated recombinant protein	Monahan et al. 2017
S3, T19, S26, S30, S37, S42, S61, S77, T78, S86, S87, S95, S96, T109, S110, S112, S115, S117	IP & mass spec – calicheamicin-treated H4 neuroglioma cells	**This study**
S3, S26, T71, S77, S96	IP & mass spec – calicheamicin-treated HEK293 cells	**This study**; Monahan et al. 2017
S26, S42, S61, S84, S131	Protein sequencing - In vitro DNA-PK treated recombinant	Gardiner et al. 2008
S30	IP & mass spec – camptothecin-treated H4 neuroglioma cells	**This study**
S42	Phospho-specific antibody – ionizing & UV radiated HEK293 cells	Gardiner et al. 2008

FIGURE 1: The prionlike domain of cellular FUS contains numerous phosphorylation sites. (A) Lysates from multiple human cell lines treated with calicheamicin or calyculin-A showed FUS migrating with a larger apparent molecular weight in Western blot; HEK293T, $n = 5$; H4, $n = 4$; U-2 OS, $n = 2$. (B) Treatment of immunoprecipitated FUS with phosphatase caused FUS to return to its normal apparent size; *Heavy chain of the immunoglobulin G used for immunoprecipitation; $n = 2$. (C) Substituting glutamate at potential serine or threonine phosphorylation sites caused ectopic FUS in H4 cells to migrate similarly to endogenous FUS from cells treated with calicheamicin or calyculin-A; see *Materials and Methods* for exact substitution sites; $n = 2$. (D) Twenty-eight serines and threonines have been identified in this and other studies as putative sites of phosphorylation (bold and underlined; DNA-PK consensus sites are shown in red). Here sites were identified by mass spectrometry following immunoprecipitation of FUS from lysates of human cell lines treated with the DNA-damaging agents calicheamicin or camptothecin, or the phosphatase-inhibitor calyculin-A.

ATM was used to confirm these treatments caused a DNA-damage response (Figure 2A). Even when dosage or treatments were extended and Western blot exposures were increased, there were no definitive FUS band shifts observed, although band shadowing suggested some FUS might be running at a slightly higher molecular weight (Supplemental Figure S1B).

We concluded that calicheamicin, calyculin-A, and staurosporine were extreme in their effects on total cellular FUS and hypothesized that the other drugs might still cause FUS PrLD phosphorylation, but in a small subpopulation of FUS, or at lower frequencies on individual proteins, not revealed by a discernible band shift (Figure 2B). For these reasons, we generated polyclonal antibodies against FUS PrLD peptides encompassing phosphorylated Ser-26 or Ser-30 (Figure 2C). These peptides were chosen because phospho-Ser-26 and phospho-Ser-30 were repeatedly identified by our mass spectrometry experiments. Immunoblotting of phosphorylated and unphosphorylated synthetic peptides with the anti-FUS(pSer26) and anti-FUS(pSer30) antibodies indicated their specificity (Figure 2C). In Western blots with calyculin-A– or calicheamicin-treated HEK293T cell lysates, the antibodies recognized a protein species at the same position as commercial FUS antibody (Figure 2B). The phospho-specific antibodies did not recognize species from untreated controls. In all Western blots, there was a direct relationship between FUS protein band shift and phospho-specific antibody recognition (Figures 2 and 3 and Supplemental Figure S1, A, C, D, and F). Small interfering RNA (siRNA) knockdown was performed to ensure the custom antibodies were specific to FUS (Figure 2, D and E, and Supplemental Figure S3).

Because FUS-linked pathology presents in neurons, we chose to continue all experiments in the H4 cell type as it is neuronal in origin. Administering a dose series of calicheamicin to H4 cells revealed that at lower concentrations anti-FUS(pSer26) and anti-FUS(pSer30) recognize a subpopulation of FUS prior to an increase in apparent molecular weight by Western blot (Figure 3A). This confirmed that phosphorylation could occur at lower levels without an obvious band shift. We next looked specifically for low levels of phosphorylation after treating H4 cells with etoposide, camptothecin, doxorubicin, bleomycin, UV radiation, and ionizing

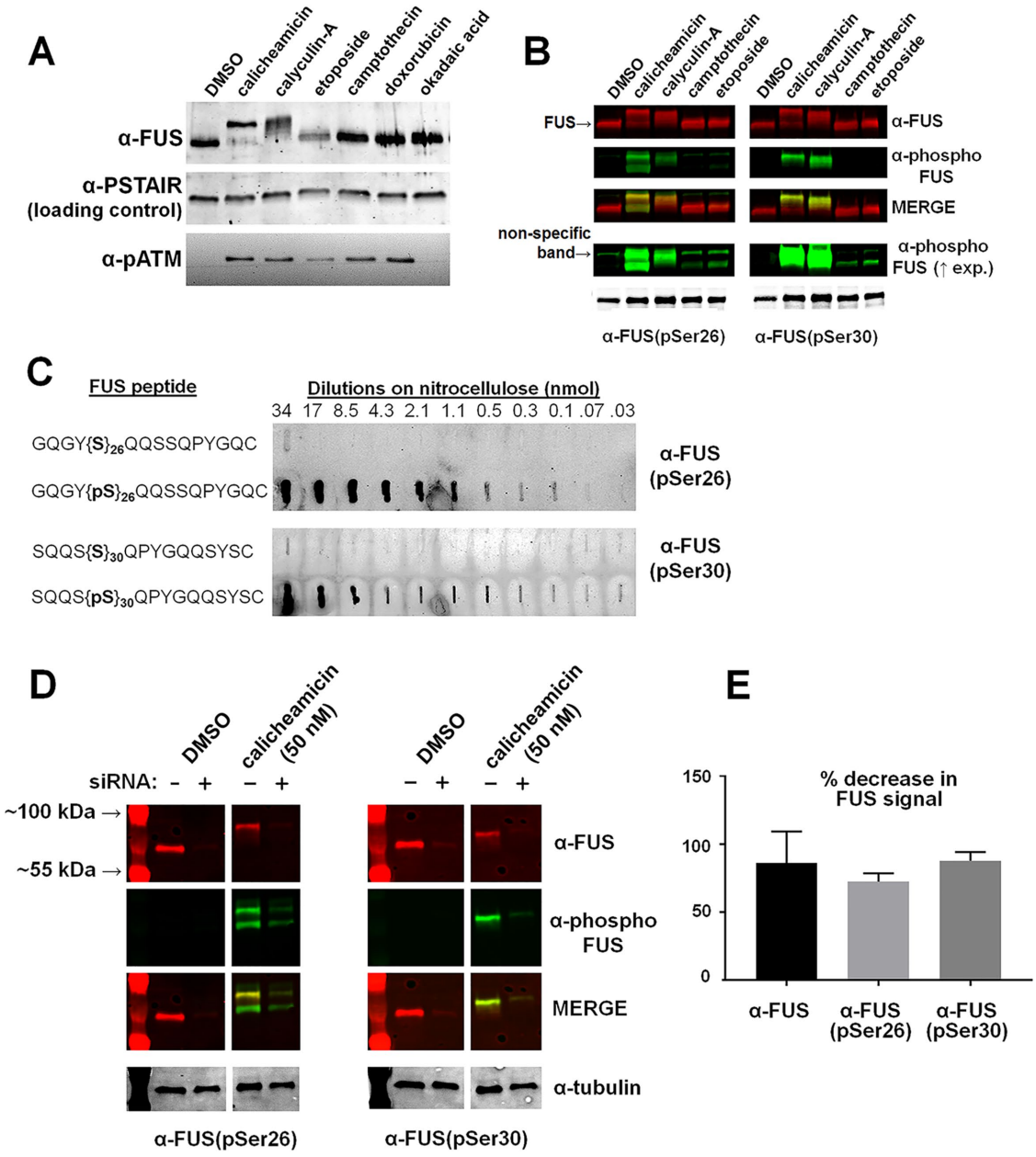

FIGURE 2: Custom anti-FUS(pSer26) and anti-FUS(pSer30) antibodies are specific to phosphorylated FUS. (A, B) Lysates of HEK293T cells treated with various reagents (DMSO, 50 nM calicheamicin, 100 nM calyculin-A, 200 μM etoposide, 10 μM camptothecin, 2 μM doxorubicin, or 100 nM okadaic acid) for 3 h at 37°C were analyzed by Western blotting with commercial FUS or with anti-FUS(pSer26) or anti-FUS(pSer30) antibodies, respectively; $n = 2$. (C) Phosphorylated and unphosphorylated synthetic peptides—corresponding to regions within FUS's prionlike domain—were serially diluted, spotted on nitrocellulose, and immunoprobed with custom antibodies: anti-FUS(pSer26) or anti-FUS(pSer30); $n = 2$. (D) FUS was knocked down using siRNA in H4 cells then treated with calicheamicin (or DMSO; negative control) to induce phosphorylation. Western blots using anti-FUS(pSer26), anti-FUS(pSer30), and commercial FUS antibodies revealed specificity of the phosphoantibodies to the FUS protein; $n = 4$. (E) Densitometry analysis of the percentage of signal reduction with FUS knockdown compared with the control; error bars represent 95% confidence intervals.

radiation (IR). These treatments are known to induce DNA damage through different mechanisms (Povirk, 1996; Liu *et al.*, 2000; Rastogi *et al.*, 2010; Yang *et al.*, 2014a; Montecucco *et al.*, 2015; Xu and Her, 2015; Mavragani *et al.*, 2017). However, each results in the production of double-strand DNA breaks that induce the DNA damage response pathway involving both ATM and DNA-PK (Shrivastav *et al.*, 2008). All treatments caused FUS phosphorylation without a pronounced concomitant band shift (Figure 3, B and C; and in HEK293T cells shown in Supplemental Figure S1, C, D, and F). Of note, low concentrations of calyculin-A (5 vs. 100 nM) and UV radiation reproducibly caused observable phosphorylation at Ser-30 but not Ser-26. In control experiments with synthetic peptides, anti-FUS(pSer26) appeared more sensitive in epitope recognition than anti-FUS(pSer30), and its specificity was not diminished by diphosphorylation at both positions 26 and 30 (Figure 2C and Supplemental Figure S1E). For these reasons, we

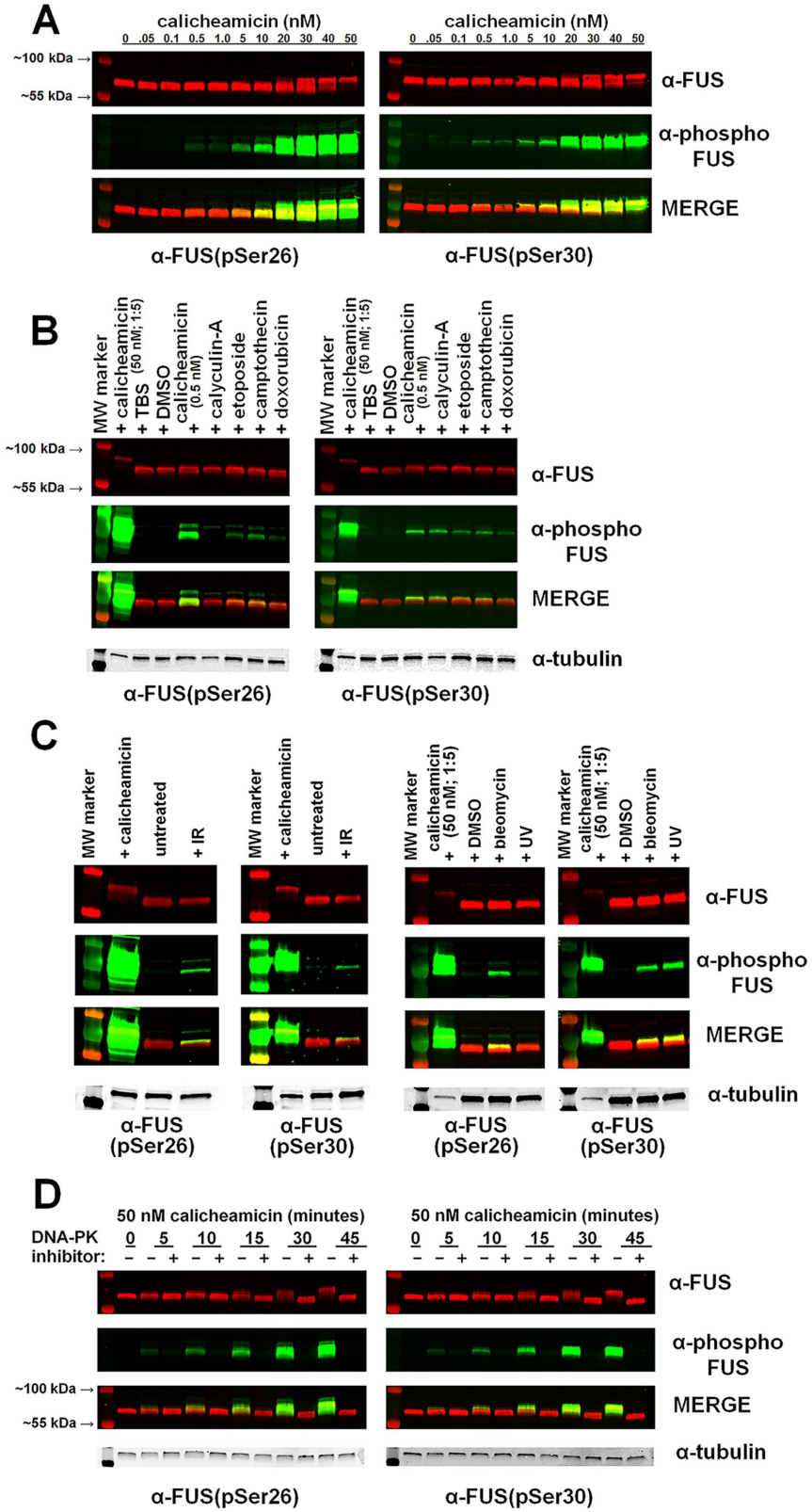

FIGURE 3: DNA-damaging conditions result in phosphorylation of Ser-26 and -30 of FUS. (A) Lysates of H4 cells treated with increasing amounts of calicheamicin were analyzed by Western blotting with commercial FUS and anti-FUS(pSer26) or anti-FUS(pSer30) antibodies; $n = 2$. (B, C) Lysates of H4 cells subjected to DNA-damaging conditions (0.5 nM calicheamicin, 5 nM calyculin-A, 200 μM etoposide, 10 μM camptothecin, 2 μM doxorubicin, 100 nM BLM, 90 mJ UV, or 20 Gy IR) were analyzed by Western blotting with commercial FUS and anti-FUS(pSer26) or anti-FUS(pSer30) antibodies; $n = 3$ for each treatment except IR in which $n = 2$. (D) Lysates of H4 cells treated with and without DNA-PK inhibitor (NU7441) prior to calicheamicin treatment were analyzed by Western blotting with commercial FUS and anti-FUS(pSer26) or anti-FUS(pSer30) antibodies; $n = 3$.

concluded differential phosphorylation is occurring in cells and is not a probing artifact.

As mentioned above, DNA-PK was previously implicated in the phosphorylation of FUS following DNA-damaging stress (Deng *et al.*, 2014). When we treated cells with the DNA-PK inhibitor NU7441 followed by calicheamicin, the FUS band shift was completely eliminated, and the phospho-specific antibodies no longer recognized any FUS species (Figure 3D). This corroborates DNA-PK's involvement in FUS PrLD phosphorylation.

FUS remains nuclear following PrLD phosphorylation induced by DNA damage

It was previously suggested phosphorylation of the FUS PrLD following a DNA damage response could potentiate pathological aggregation by promoting FUS's cytoplasmic localization (Deng *et al.*, 2014). Alternatively, in previous work, we found phosphorylation of the PrLD might be protective since it disfavors LLPS and aggregation (Monahan *et al.*, 2017). We used phospho-specific and non–phospho-specific FUS antibodies to evaluate the relationship between DNA damaging stress, FUS phosphorylation, and FUS localization.

Immunofluorescence microscopy of H4 cells revealed total cellular FUS remained unchanged in its nuclear localization following treatment with the DNA-damaging agents calicheamicin, camptothecin, and etoposide (Figure 4A). Treatment caused nuclear phospho-FUS (at Ser-30) to appear within ~15 min and persist in the nucleus for over an hour (Figure 4A). The same pattern was observed in U-2 OS and HEK293T cells (Supplemental Figure S4, A and B). To determine whether the extent of phosphorylation could alter FUS localization, we used low and high calicheamicin concentrations to cause lower and higher levels of phosphorylation, respectively. With both treatments, FUS remained nuclear like untreated controls (Figure 4A). Localization experiments were performed using anti-FUS(pSer30) because it revealed less nonspecific binding in siRNA immunofluorescence microscopy experiments (Figure 4, B and C).

Unlike the effects of the DNA-damaging agents, we observed calyculin-A and staurosporine to cause various levels of FUS phosphorylation and cytoplasmic localization (Supplemental Figure S4, A and C). However, both treatments dramatically altered cell morphology and caused adherent cells to disperse in culture. These effects were reproducible over multiple cell types and

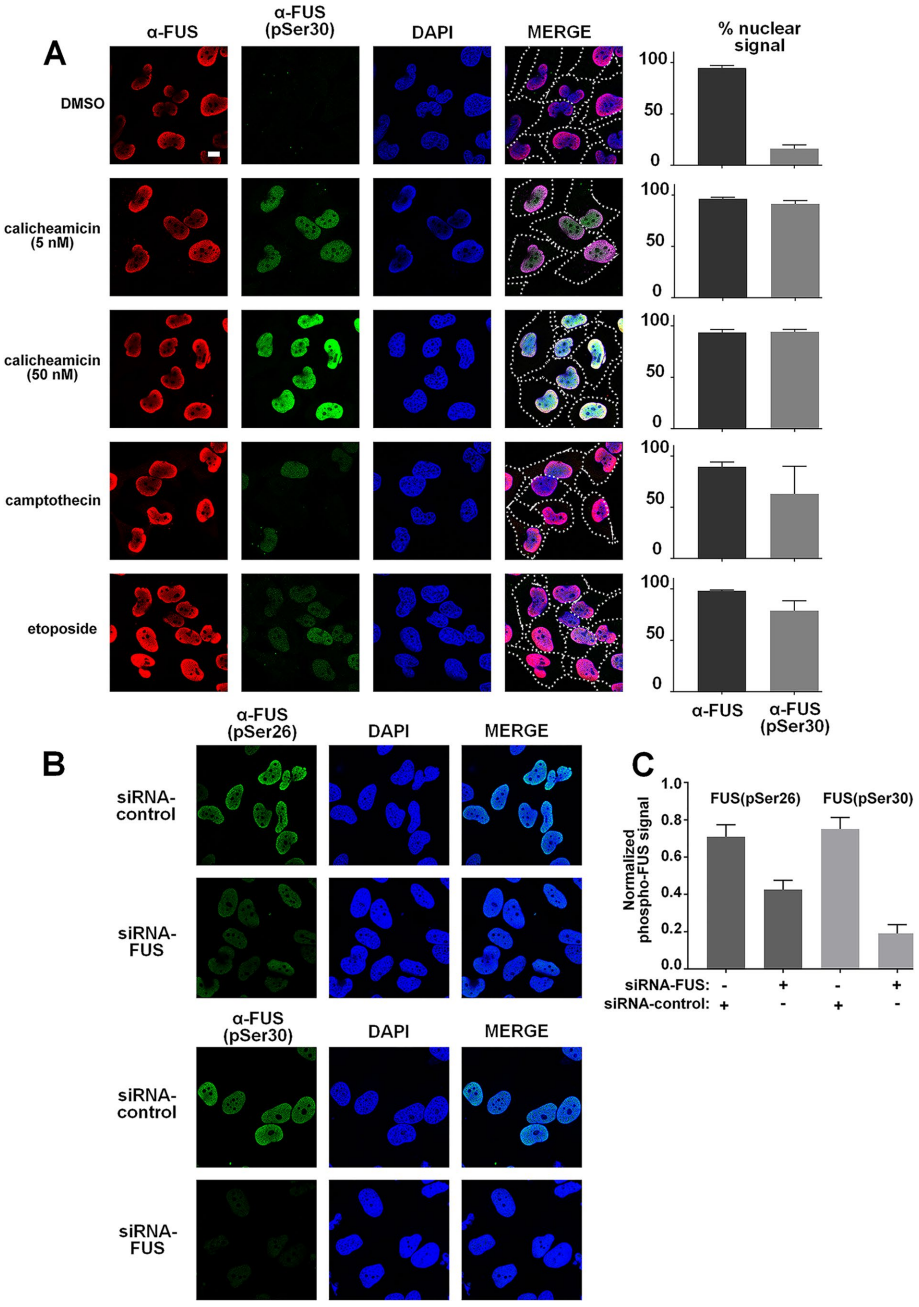

FIGURE 4: FUS remains nuclear following DNA-PK–dependent phosphorylation at Ser-30. (A) H4 cells were fixed for immunocytochemical analysis using commercial FUS and anti-FUS(pSer30) antibodies following treatment with DNA-damaging agents (DMSO, 50 or 5 nM calicheamicin, 60 μM camptothecin, 100 μM etoposide); quantification of nuclear and cytoplasmic fluorescence was used to determine the percentage of total FUS in the nucleus per cell; error bars represent 95% confidence intervals; the anti-FUS(pSer30) signal quantified in DMSO-treated cells resulting in ~20% nuclear localization is due to background fluorescence; $n = 3$. (B, C) siRNA knockdown of FUS in H4 cells, using FUS-specific and scrambled-control nucleotides, showed a significant reduction in nuclear signal when cells were probed with both anti-FUS(pSer26) and anti-FUS(pSer30); error bars represent a 95% confidence interval; $n = 3$.

not observed with other treatments (Supplemental Figure S4, A and C). When we further evaluated FUS localization after staurosporine treatment, we observed phospho-FUS only in the nuclei and never in the cytoplasm (Supplemental Figure S4C).

As a positive control for FUS cytoplasmic localization, we subjected cells to osmotic stress, which was previously shown to cause an increase in cytoplasmic localization of FUS (Sama *et al.*, 2013). Cytoplasmic localization was reported to depend on dimethylation of FUS arginine residues within its arginine-/glycine-rich domains. Using sorbitol (0.4 M), we confirmed osmotic stress causes FUS to rapidly localize to the cytoplasm (Supplmental Figure S5A). We also confirmed that FUS arginine dimethylation is required for cytoplasmic localization; when the methylase inhibitor adenosine-dialdehyde (Adox) was added, FUS remained nuclear following osmotic stress (Supplemental Figure S5, A and B). Theoretically, some of the DNA-damaging conditions we used could have simultaneously affected FUS arginine methylation, which would confound experiments that evaluate FUS localization. However, we found no evidence the experimental conditions that caused FUS phosphorylation were simultaneously affecting FUS's arginine dimethylation (Supplemental Figure S5, C and D).

DNA-PK–dependent phosphorylation of the PrLD does not promote FUS cytoplasmic localization

We asked whether PrLD multiphosphorylation has any effect on the change in localization of FUS induced by osmotic stress. H4 cells were treated with calicheamicin to induce phosphorylation and then subjected to osmotic stress with sorbitol. Using immunofluorescence microscopy, accumulation of total FUS in the cytoplasm appeared slightly inhibited in the calicheamicin-treated cells relative to control cells over time (Figure 5A). The FUS band shift in the Western blot suggested that FUS was multiphosphorylated under these conditions (Figure 5B). Next, using the phospho-specific anti-FUS(pSer30) antibody, the experiment was repeated with an extended end point. As before, the addition of calicheamicin prior to sorbitol resulted in a modest, but statistically significant, reduction of FUS in the cytoplasm (Figure 5, C and E). However, phosphorylated FUS was only observed in the nucleus of calicheamicin-treated cells—never in the cytoplasm. Likewise, we found that adding calicheamicin after sorbitol resulted in the rapid appearance of phosphorylated FUS only in the nucleus and not in the cytoplasm (Figure 5, C and E). This is consistent with DNA-PK's nuclear localization and activity (Anderson and Lees-Miller, 1992). Western blot controls confirming FUS phosphorylation are shown in Figure 5D, and extended immunofluorescence control images are shown in Supplemental Figure S6. Similar nuclear-only localization of phospho-FUS was observed using the anti-FUS(pSer26) antibody (Supplemental Figure S7).

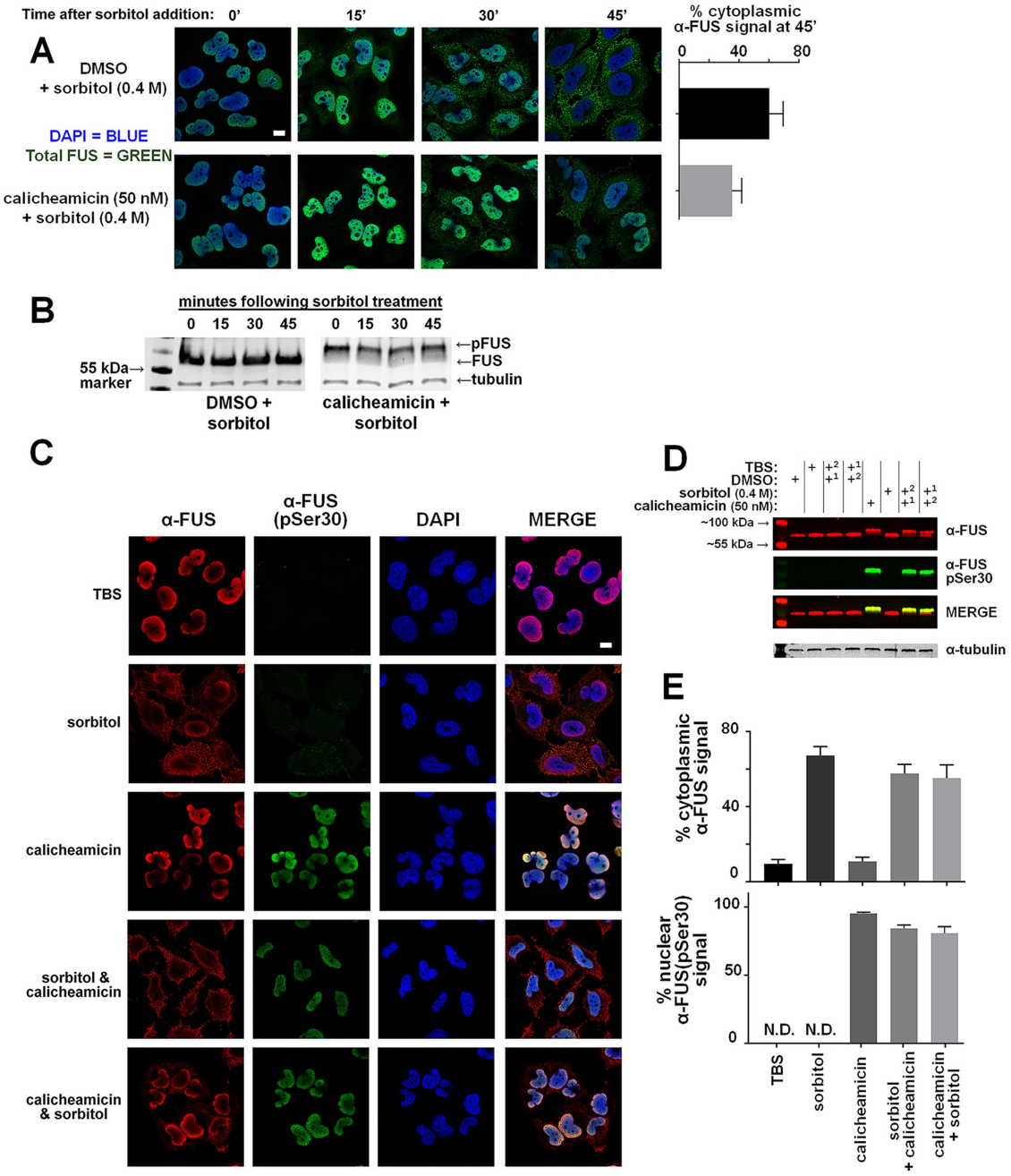

FIGURE 5: Calicheamicin-induced phosphorylated FUS is maintained in the nucleus following osmotic stress. (A) H4 cells treated with 0.4 M sorbitol, with and without 50 nM calicheamicin pretreatment, were fixed for immunocytochemical analysis with a commercial FUS antibody; nuclear and cytoplasmic fluorescence signals at the 45-min time point were quantified to determine the percentage of total FUS in the cytoplasm per cell (right panel); error bars represent 95% confidence intervals; $n = 3$. (B) Lysates were analyzed by Western blotting; $n = 2$. (C) H4 cells were fixed for immunocytochemical analysis with commercial FUS and anti-FUS(pSer30) antibodies following sequential addition of sorbitol and/or calicheamicin (60 min sorbitol before 60 min calicheamicin, or 60 min calicheamcin before 60 min sorbitol, without removal of the first treatment); $n = 3$. (D) Lysates were analyzed by Western blotting; $n = 3$. (E) Quantification of nuclear and cytoplasmic fluorescence signals was done to determine the percentage of total FUS in the cytoplasm per cell and the percentage of total phospho-FUS in the nucleus per cell (N.D. = not determined); error bars represent 95% confidence intervals.

We next asked how inhibition of DNA-PK could alter the balance between nuclear and cytoplasmic FUS. When H4 cells were treated with the DNA-PK inhibitor NU7441, we observed no effect on FUS localization. However, if cells were subjected to calicheamicin after treatment with the inhibitor, the majority of FUS localized to the cytoplasm (Figure 6, A and B). Figure 6C shows Western blots confirming the efficacy of calicheamicin and inhibitor. The data suggest that neither DNA-PK activity nor PrLD phosphorylation at positions 26 and 30 is sufficient to drive FUS cytoplasmic localization.

Because the entire FUS PTM repertoire that follows calicheamicin treatment is unknown and is not necessarily limited to PrLD modifications, it is possible that PrLD phosphorylation favors

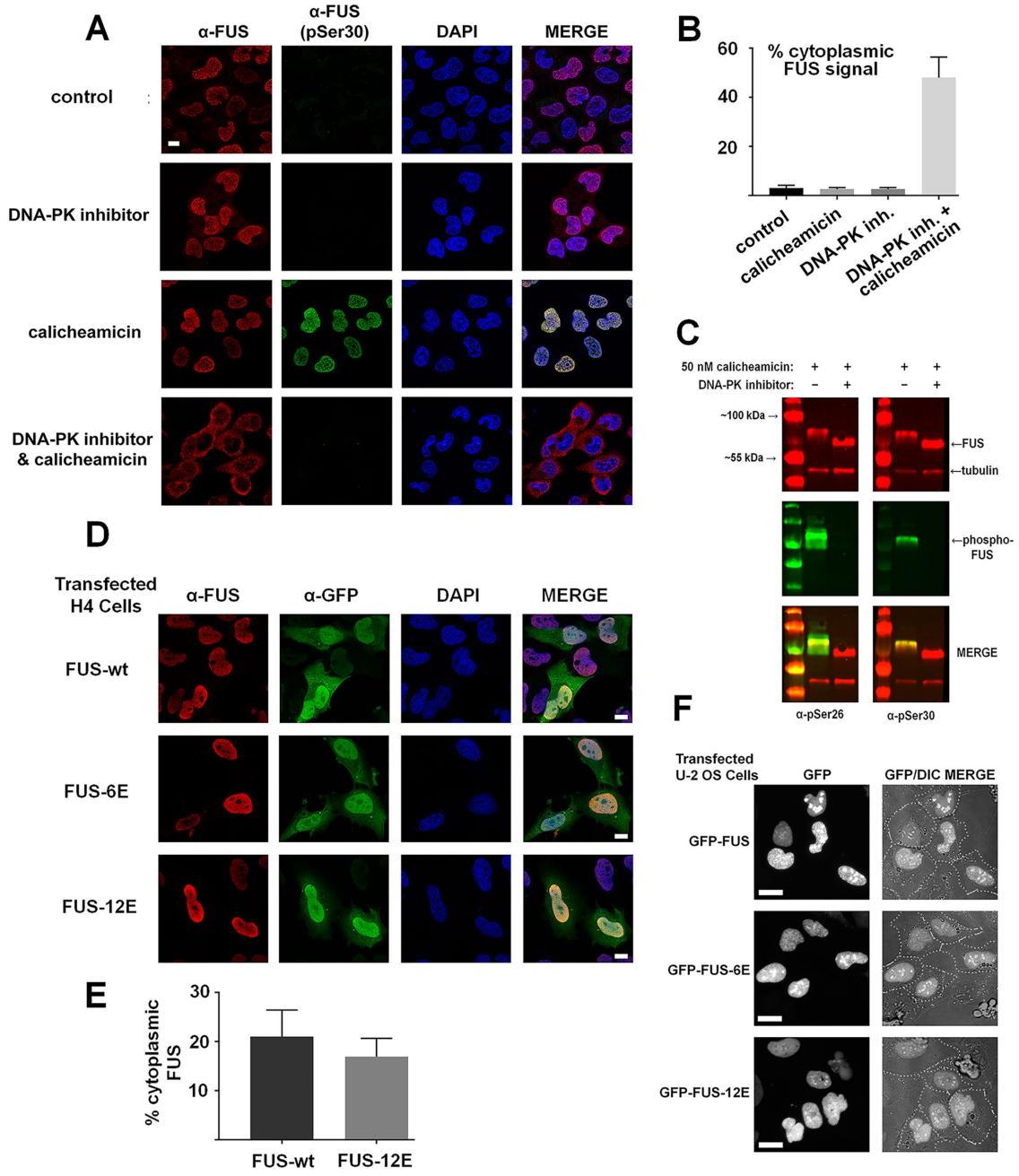

FIGURE 6: Phosphorylation of the FUS prionlike domain is not linked to cytoplasmic localization. (A) H4 cells following calicheamicin treatment, with and without DNA-PK inhibitor (NU7441), were fixed for immunocytochemical analysis using commercial FUS and anti-FUS(pSer30) antibodies; $n = 3$. (B) Quantification of nuclear and cytoplasmic fluorescence signals was done to determine the percentage of cytoplasmic localization; error bars represent 95% confidence interval. (C) Lysates were analyzed by Western blotting; $n = 3$. (D) H4 cells expressing ectopic PM FUS (6 or 12 glutamate substitutions in the prionlike domain) were visualized by immunofluorescence microscopy; $n = 3$. (E) Quantification of nuclear and cytoplasmic fluorescence signal was done to determine the percentage of cytoplasmic localization of FUS-wt and FUS-12E from C; error bars represent 95% confidence intervals. (F) U-2 OS cells expressing GFP-fused ectopic phosphomimetic FUS were visualized by live-cell imaging; $n = 2$.

cytoplasmic localization but is masked by other PTMs. We used H4 cells and a dual-expression plasmid system that expresses GFP and FUS phosphomimetic variants as separate proteins. The FUS variants were specifically modified at DNA-PK sites within the PrLD to determine their effects on FUS subcellular localization (phosphomimetics discussed in Figure 1C and Supplemental Figure S8; see *Materials and Methods* for sites). GFP fluorescence was used to determine which transfected cells expressed ectopic proteins at similar levels. The localization of ectopic FUS, FUS-6E, or FUS-12E was evaluated by immunofluorescence microscopy. We found that FUS, FUS-6E, and FUS-12E were all mostly nuclear (Figure 6D). Quantification yielded no significant differences in localization (Figure 6E). A similar experiment was performed in live U-2 OS cells expressing ectopic GFP-FUS fusion proteins. Again, no difference in localization was observed by introducing phosphomimetic substitutions (Figure 6F).

DISCUSSION

The results of our mass spectrometry experiments suggest that extensive FUS PrLD phosphorylation can occur in cells: Twenty-eight putative sites identified to date, which represents ~17% of the approximately 160-amino-acid domain. In combination with the characteristic molecular weight shift of the FUS protein band in Western blots, it can be inferred that multiphosphorylation of the PrLD is occurring under certain cellular conditions. Here we confirmed phosphorylation of two of the predicted DNA-PK consensus sites (Ser-26 and Ser-30) within the PrLD using human cell lines under DNA-damaging stress. Previously, Gardiner *et al.* (2008) identified Ser-42 phosphorylation under similar conditions; thus, three of the 12 DNA-PK motifs in the PrLD have been confirmed as sites of phosphorylation in cells. This suggests many of the other predicted sites may also be phosphorylated in cells.

If a moderate fraction of the predicted phosphorylation sites within the FUS PrLD are phosphorylated, then the PrLD will fail—by definition—to preserve its prionlike character. Canonical prion domains are inherently low-complexity, consisting of mostly nonaliphatic and noncharged amino acids. All PrLD's share these compositional features. Moreover, they are frequently found in proteins that pathologically aggregate in neurons (Gitler and Shorter, 2011) or undergo LLPS. The FUS PrLD contributes to both phenomena: it strongly enhances FUS's aggregation propensity in cells (Kryndushkin *et al.*, 2011) and it is critical to FUS's ability to undergo LLPS (Burke *et al.*, 2015). Both phenomena depend on protein self-association and, in this regard, are reminiscent of yeast prion behavior. Since FUS's PrLD is considered integral to both LLPS and solid aggregate formation, the decrease in prionlike character through multiphosphorylation may have dramatic effects on FUS's cellular behavior.

Murray and coworkers discovered, in vitro, that FUS PrLD forms archetypical amyloid fibers with parallel in-register cross-beta architecture (Murray *et al.*, 2017). This type of structure explains how aggregated proteins can pathologically propagate similarly to yeast prions (Shewmaker *et al.*, 2006). Eleven of the identified putative phosphorylation sites are located within the core of Murray's predicted FUS amyloid fibers (amino acids 39–95). Because the individual proteins align in-register to form the amyloid core, the introduction of multiple charges via phosphates would be structurally unfavorable due to electrostatic repulsion. Consistent with this idea, we previously found dramatic qualitative effects on FUS aggregation and toxicity in cell models with ~4–6 PrLD phosphomimetic substitutions (Monahan *et al.*, 2017). Based on our observations here, manipulation of cellular phosphatases and kinases could provide a realistic mechanism to combat FUS aggregation through multiphosphorylation.

Multiphosphorylation may also regulate FUS incorporation into phase-separated ribonucleoprotein granules in cells. Recombinant FUS PrLD remains structurally disordered in the phase-separated state (Burke *et al.*, 2015). However, the cross-beta in-register interactions found in the solid state were hypothesized to be similar to the dynamic interactions that may occur in the phase-separated state (Murray *et al.*, 2017). In this scenario, multiphosphorylation may hinder LLPS similarly to how it disfavors solid aggregate formation: primarily through electrostatic repulsion. We previously observed dramatic qualitative effects on LLPS in vitro with six phosphomimetic substitutions, though fewer were not tested (Monahan *et al.*, 2017). In agreement with our findings, Lin and coworkers modeled phase separation using an experimental system with SH3 domain protein. When the FUS PrLD was fused to SH3, the system underwent LLPS at lower concentration. However, DNA-PK treatment (i.e., phosphorylation) resulted in dissolution of the droplets (Lin *et al.*, 2017). These results suggest a mechanism by which FUS function, interactions, and localization could be regulated rapidly under physiologic and stress conditions.

Previously, DNA-PK–dependent phosphorylation of the PrLD was suggested to facilitate FUS nuclear export (Deng *et al.*, 2014). This was a significant finding because cytoplasmic accumulation may potentiate pathology. However, this observed cytoplasmic localization could be due to particularities of the drugs used in the study: calyculin-A and staurosporine. Calyculin-A is a phosphatase-inhibitor and staurosporine is a kinase inhibitor. Neither are specifically DNA-damaging agents and both induce apoptosis (Stepczynska *et al.*, 2001; Kleppe *et al.*, 2015), so for these reasons we did not further pursue their effects here. However, since both drugs were previously used to characterize FUS localization, they could have influenced conclusions. Understandably, we and others use these potent drugs because they easily enable the study of FUS PrLD phosphorylation, but their full individual effects on cellular mechanisms and other FUS domains may yield different experimental results.

Under osmotic stress conditions, we recapitulated previous observations that arginine dimethylation is critical to cytoplasmic localization of FUS (Dormann *et al.*, 2012; Sama *et al.*, 2013; Scaramuzzino *et al.*, 2013). We determined the treatments that induce FUS phosphorylation do not appear to impact arginine dimethylation, which is a conceivable mechanism by which they could indirectly govern nucleocytoplasmic localization. To determine whether PrLD phosphorylation alone could cause cytoplasmic localization, we examined the localization of ectopically expressed phosphomimetic FUS. Assuming the S/T-to-E substitutions mimic the effects of phosphorylation, we concluded that phosphorylation of DNA-PK consensus sites in the PrLD is not sufficient to cause FUS cytoplasmic localization. Thus, FUS's arginine dimethylation status is directly linked to its subcellular localization, while no similar link currently exists for FUS PrLD phosphorylation.

DNA-PK is activated by double-strand DNA breaks. When cells are treated with calicheamicin, the DNA-PK–dependent phosphorylation of FUS is robust. However, extensive phosphorylation (or phosphomimetic substitution) of the PrLD does not change FUS's subcellular localization. Retention of FUS in the nucleus following DNA damage would be consistent with FUS having a critical nuclear activity. Thus, DNA-PK–dependent FUS phosphorylation following DNA damage, corroborates FUS's proposed function in the DNA damage response pathway. This is supported by the repertoire of DNA damaging treatments we confirmed to induce low levels of phosphorylation and still maintain nuclear localization. The change in localization that occurs when DNA-PK is inhibited prior to calicheamicin treatment suggests PrLD phosphorylation may be causing a retention of FUS to the nucleus. Validation of this prediction and elucidation of the mechanism by which this may be occurring is undetermined and necessitates further research.

The generation of phospho-specific FUS antibodies confirmed Ser-26 and Ser-30 phosphorylation following DNA damaging stress but generally only in a small percentage of total cellular FUS. Since FUS is implicated in many diverse functions, the entire cellular population may not require identical PTMs, which is consistent with our observation that subpopulations of FUS show differential levels of phosphorylation. For example, we observed situations in which Ser-30 phosphorylation appeared in the absence of Ser-26 phosphorylation. This was especially pronounced with UV radiation. For comparison, Gardiner *et al.* found phosphorylation of Ser-42 was noticeably stronger following IR stress compared with other DNA-damaging conditions (Gardiner *et al.*, 2008). Thus, different responses and

activities may require a specific pattern of PTMs. Likewise, 20 or more arginine residues of FUS are proposed to be mono- or dimethylated under various conditions (Rappsilber *et al.*, 2003); how precisely this governs specific subcellular localization remains unknown, but a huge mathematical combination of potential PTMs exists. We observed rapid relocalization of FUS after calicheamicin treatment when DNA-PK was inhibited, despite no evidence of PrLD phosphorylation. Again, specific PTMs beyond DNA-PK phosphorylation may underlie this localization response and will require further study.

MATERIALS AND METHODS

Cell culture

H4 neuroglioma (ATCC HTB-148) and HEK293T (ATCC CRL-11268) cells were cultured in DMEM-based media (Sigma D6429) supplemented with 10% fetal bovine serum (FBS) (Sigma-Aldrich F6178) and 1% penicillin–streptomycin (Corning 30-002-CI) or 1% penicillin–streptomycin–glutamine (Corning 30-009-CI), respectively. U-2 OS cells (ATCC HTB-96) were cultured in McCoy 5A based media (Lonza 12-688F) supplemented with 10% FBS and 1% penicillin–streptomycin. Cells were lysed by resuspension and incubation in lysis buffer (200 mM NaCl,100 mM Tris-HCl, 0.5% sodium deoxycholate, 1% Triton X-100, 0.2% SDS, 660 mM phenylmethylsulfonyl fluoride, 100 µl protease inhibitor cocktail (Sigma P8215), 100 µl phosphatase inhibitor cocktail (Sigma P0044), 1250 U Benzonase nuclease) while on ice.

The following drugs were used to treat the human cell lines: calicheamicin-γ (a generous gift from Pfizer), calyculin-A (Sigma C5552), camptothecin (Sigma C9911), etoposide (Sigma E1383), doxorubicin (Cayman Chemical 15007), okadaic acid (Sigma O9381), bleomycin (Cayman Chemical 13877), DMSO (Sigma D8418), DNA-PK inhibitor (Selleckchem NU7441), sorbitol (Sigma A1876), and Adox (Sigma A7154). UV irradiation was carried out by a standard germicidal ultraviolet light with 95% of the ultraviolet radiation in the 254-nm region at 37°C. Ionizing radiation exposures were performed under 34 Gy/h in a ^{137}Cs irradiator (GammaCell 40; J. L. Shepard and Associates) at 30°C. All drug treatments or radiation exposures were carried out for 1 h at 37°C unless otherwise specified.

Western blotting and immunoprecipitation

Cell lysates were mixed with 4X NuPAGE LDS Sample Buffer (Thermo Fisher NP0008) and run through SDS–PAGE using precast gels (Bio-Rad 456-9034). Protein was transferred onto nitrocellulose membrane (Bio-Rad 162-0146) using the Trans-Blot Turbo Transfer System (Bio-Rad 170-4150). Membranes were blocked in 6% milk (Bio-Rad 1706404XTU) in Tris-buffered saline (TBS) with 0.1% Tween-20 or Odyssey Blocking Buffer (LI-COR 927-40000). Primary and secondary antibodies were diluted in phosphate-buffered saline with 0.1% Tween-20. Secondary antibodies were conjugated to IRDye fluorochromes (LI-COR 926-32211; 925-68020), and their fluorescence was detected using the Odyssey LCx Imaging System (LI-COR). Biological replicates (*n*) were produced from separately cultured cells. Densitometry analysis was done using the Odyssey LI-COR Image Studio program. All data were displayed as the mean value with error bars representing 95% confidence intervals, unless otherwise stated in the figure legends, using GraphPad Prism version 7.00 for Windows (GraphPad Software, La Jolla, CA, www.graphpad.com).

Protein G–conjugated Dynabeads (Invitrogen 10007D) and 5 µg of antibody were used to immunoprecipitate FUS from mammalian cell lysates following the manufacturer's protocol. The following FUS antibodies were used: Bethyl A300-293A and custom-produced rabbit anti-FUS(Ser-30) phosphorylated and unphosphorylated peptides (PAN).

Immunocytochemistry and ImageJ quantification

Cells were grown on glass coverslips for 24 h prior to indicated treatments and fixation with 4% paraformaldehyde (Sigma-Aldrich P6148). The fixed cells were permeabilized in –20°C methanol and blocked in 5% normal goat serum containing 0.05% sodium azide (Life Technologies 50062Z) in preparation for immunostaining. Mouse anti-FUS (Santa Cruz 373698) and custom-produced rabbit antibodies against phosphorylated FUS (Genscript) antibodies were used as primary antibodies to probe the fixed cells. AF488 and AF586 conjugated secondary antibodies (Southern Biotech 1030-30; Life Technologies A11011) were used to detect the primary antibodies, and DAPI-containing mounting media (Invitrogen P36931) was used to stain the nuclei and mount the coverslips to glass slides. The Zeiss 700 confocal microscope was used to view and image the prepared slides. Biological replicates (*n*) were produced from separately cultured cells.

Quantification was performed using Fiji (Schindelin *et al.*, 2012). For each immunofluorescence microscopy image shown, between 5 and 10 cells were quantified per biological replicate for statistical analysis. Quantification of subcellular localization was done using the Raw Integrated Density measurement. Nuclear and cytoplasmic areas were mapped under the highest maximum threshold setting and a minimum threshold setting of 10 and 1, respectively. Quantitative measurements were made without applied thresholds. Knockdown experiments were quantified using the mean gray value measurement with the same mapping techniques. All data are displayed as the mean value with error bars representing 95% confidence intervals using GraphPad Prism version 7.00 for Windows (GraphPad Software).

Phosphatase treatment of FUS protein

Immunoprecipitated FUS was treated with calf intestinal phosphatase (CIP; NEB M0290L) in a reaction buffer (100 mM NaCl, 50 mM Tris-HCl pH 8, 10 mM $MgCl_2$, 1 mM dithiothreitol (DTT), 1 EDTA-free protease inhibitor tablet (1 tablet per 5 ml of solution; Roche 11873580001)) at 37°C for 90 min. Mock treatment contained the reaction buffer without the enzyme. The resulting reactions were separated by SDS–PAGE for Western blot analysis.

Plasmids, knockdown, and mammalian cell transfection

Wild-type FUS and its phosphomimetic variants were subcloned from pET vectors previously constructed (Monahan *et al.*, 2017) into both mEGFP-C1 (Addgene 54759) and pIRES2-EGFP-SHP2DA (Addgene 12286) using *Bam*HI/*Xho*I restriction sites. The phosphomimetic substitution in each construct are listed below. Plasmid DNA was transfected into cell lines using OptiMEM (Life Technologies 31985-070) transfection medium and Lipofectamine 2000 (Thermo Fisher 11668027) at a ratio of 0.5 µg: 2.5 µl (DNA: Lipofectamine 2000). Transfection mixture was diluted 1:4 into complete cell media and incubated at 37°C for 8–10 h.

Phosphomimetic substitutions in FUS are diagrammed in Supplemental Figure S8 and are as follows: FUS-1E (T19E); FUS-3E (S26E, S30E, T68E); FUS-4E (T68E, S84E, S87E, S117E); FUS-6E (S26E, S30E, T68E, S84E, S87E, S117E); FUS-12E (T7E, T11E, T19E, S26E, S30E, S42E, S61E, T68E, S84E, S87E, S117E S131E).

Custom peptide and antibody production and testing

Pairs of phosphorylated and nonphosphorylated peptides were synthesized corresponding to FUS residues 22–36 (GQGYSQQSSQ-PYGQQ; Ser-26 underlined) and residues 26–40 (SQQSSQPYGQQ-SYSG; Ser-30 underlined). The phosphorylated peptides were used as immunogens for antibody production in rabbits. Following

immunological challenge with each phosphopeptide, antibodies specific to the phosphorylated peptides were purified: anti-FUS(pSer26) and anti-FUS(pSer30). Nonspecific antibodies that recognized both PAN were also isolated. Peptide synthesis and antibody production were performed by Genscript (Piscataway, NJ).

Phosphorylated and nonphosphorylated peptides were blotted onto nitrocellulose and probed with anti-FUS(pSer26) and anti-FUS(pSer30) antibodies following normal Western blotting protocols. Knockdown of FUS from H4 cells using Lipofectamine RNAiMAX (ThermoFisher 13778030) and Silencer Select siRNA specific to FUS (ThermoFisher 4392420 and 4390843) was done following manufacturer's protocol to confirm antibody specificity in cells.

Mass spectrometry

H4 cells were treated with 50 nM calicheamicin or 30 μM camptothecin for 1 h at 37°C and then lysed in nondenaturing lysis buffer (described above). FUS was immunoprecipitated (procedure described above) from the samples using protein G–conjugated Dynabeads (Invitrogen) and the custom produced polyclonal anti-FUS(Ser-30) PAN antibody (Genscript), which recognizes both phosphorylated and unphosphorylated FUS. Samples were enriched for the phosphorylated population of FUS using a titanium dioxide column (ThermoFisher Scientific). The protein was eluted, cleaved with trypsin and then chymotrypsin to isolate the N-terminal prionlike domain of FUS. Mass spectrometry analysis was then performed at the John Hopkins University Mass Spectrometry and Proteomic Facility. This protocol was previously described by Monahan and colleagues (Monahan *et al.* 2017). PEAKS Studio Software was used to view and analyze the mass spectrometry data.

ACKNOWLEDGMENTS

We thank Michael Panagos and Sarah Walsh for assistance in the laboratory, Nick Fawzi for experimental suggestions, Jesse Guidry for mass spectrometry advice, Robert Kortum for sharing immunoblotting equipment and expertise, Dennis McDaniel and Rachel Cox for help with fluorescence microscopy, Jeremy Smyth and Darya Karabasheva for sharing microscopy equipment and expertise, Jeff Harmon for reviewing the manuscript, Rok Tkavc for help with the GammaCell irradiator, and Molly Jia for her assistance in creating the custom polyclonal antibodies. Support from the National Institute of General Medical Sciences of the National Institutes of Health under Award Numbers R35GM119790 and R01GM118530 made these studies possible.

REFERENCES

Anderson CW, Lees-Miller SP (1992). The nuclear serine/threonine protein kinase DNA-PK. Crit Rev Eukaryot Gene Expr 2, 283–314.

Armstrong RA (2017). Neuronal cytoplasmic inclusions in tau, TDP-43, and FUS molecular subtypes of frontotemporal lobar degeneration share similar spatial patterns. Folia Neuropathol 55, 185–192.

Blackford AN, Jackson SP (2017). ATM, ATR, and DNA-PK: the trinity at the heart of the DNA damage response. Mol Cell 66, 801–817.

Burke KA, Janke AM, Rhine CL, Fawzi NL (2015). Residue-by-residue view of in vitro FUS granules that bind the C-terminal domain of RNA polymerase II. Mol Cell 60, 231–241.

Daigle JG, Lanson NA Jr, Smith RB, Casci I, Maltare A, Monaghan J, Nichols CD, Kryndushkin D, Shewmaker F, Pandey UB (2013). RNA-binding ability of FUS regulates neurodegeneration, cytoplasmic mislocalization and incorporation into stress granules associated with FUS carrying ALS-linked mutations. Hum Mol Genet 22, 1193–1205.

Darovic S, Prpar Mihevc S, Župunski V, Gunčar G, Štalekar M, Lee YB, Shaw CE, Rogelj B (2015). Phosphorylation of C-terminal tyrosine residue 526 in FUS impairs its nuclear import. J Cell Sci 128, 4151–4159.

Deng Q, Holler CJ, Taylor G, Hudson KF, Watkins W, Gearing M, Ito D, Murray ME, Dickson DW, Seyfried NT, Kukar T (2014). FUS is phosphorylated by DNA-PK and accumulates in the cytoplasm after DNA damage. J Neurosci 34, 7802–7813.

Devoy A, Kalmar B, Stewart M, Park H, Burke B, Noy SJ, Redhead Y, Humphrey J, Lo K, Jaeger J, *et al.* (2017). Humanized mutant FUS drives progressive motor neuron degeneration without aggregation in "FUSDelta14" knockin mice. Brain 140, 2797–2805.

Dormann D, Madl T, Valori CF, Bentmann E, Tahirovic S, Abou-Ajram C, Kremmer E, Ansorge O, Mackenzie IR, Neumann M, Haass C (2012). Arginine methylation next to the PY-NLS modulates Transportin binding and nuclear import of FUS. EMBO J 31, 4258–4275.

Fujii R, Okabe S, Urushido T, Inoue K, Yoshimura A, Tachibana T, Nishikawa T, Hicks GG, Takumi T (2005). The RNA binding protein TLS is translocated to dendritic spines by mGluR5 activation and regulates spine morphology. Curr Biol 15, 587–593.

Fujii R, Takumi T (2005). TLS facilitates transport of mRNA encoding an actin-stabilizing protein to dendritic spines. J Cell Sci 118, 5755–5765.

Gardiner M, Toth R, Vandermoere F, Morrice NA, Rouse J (2008). Identification and characterization of FUS/TLS as a new target of ATM. Biochem J 415, 297–307.

Gitler AD, Shorter J (2011). RNA-binding proteins with prion-like domains in ALS and FTLD-U, Prion 5, 179–187.

Han TW, Kato M, Xie S, Wu LC, Mirzaei H, Pei J, Chen M, Xie Y, Allen J, Xiao G, McKnight SL (2012). Cell-free formation of RNA granules: bound RNAs identify features and components of cellular assemblies. Cell 149, 768–779.

Hoell JI, Larsson E, Runge S, Nusbaum JD, Duggimpudi S, Farazi TA, Hafner M, Borkhardt A, Sander C, Tuschl T (2011). RNA targets of wild-type and mutant FET family proteins. Nat Struct Mol Biol 18, 1428–1431.

Ishigaki S, Masuda A, Fujioka Y, Iguchi Y, Katsuno M, Shibata A, Urano F, Sobue G, Ohno K (2012). Position-dependent FUS-RNA interactions regulate alternative splicing events and transcriptions. Sci Rep 2, 529.

Ishihara H, Martin BL, Brautigan DL, Karaki H, Ozaki H, Kato Y, Fusetani N, Watabe S, Hashimoto K, Uemura D (1989). Calyculin A and okadaic acid: inhibitors of protein phosphatase activity. Biochem Biophys Res Commun 159, 871–877.

Karaman MW, Herrgard S, Treiber DK, Gallant P, Atteridge CE, Campbell BT, Chan KW, Ciceri P, Davis MI, Edeen PT, *et al.* (2008). A quantitative analysis of kinase inhibitor selectivity. Nat Biotechnol 26, 127–132.

Kino Y, Washizu C, Aquilanti E, Okuno M, Kurosawa M, Yamada M, Doi H, Nukina N (2011). Intracellular localization and splicing regulation of FUS/TLS are variably affected by amyotrophic lateral sclerosis-linked mutations. Nucleic Acids Res 39, 2781–2798.

Kleppe R, Herfindal L, Døskeland SO (2015). Cell death inducing microbial protein phosphatase inhibitors—mechanisms of action. Mar Drugs 13, 6505–6520.

Kryndushkin D, Wickner RB, Shewmaker F (2011). FUS/TLS forms cytoplasmic aggregates, inhibits cell growth and interacts with TDP-43 in a yeast model of amyotrophic lateral sclerosis. Protein Cell 2, 223–36.

Kwiatkowski TJ Jr, Bosco DA, Leclerc AL, Tamrazian E, Vanderburg CR, Russ C, Davis A, Gilchrist J, Kasarskis EJ, Munsat T, Valdmanis P, *et al.* (2009). Mutations in the FUS/TLS gene on chromosome 16 cause familial amyotrophic lateral sclerosis. Science 323, 1205–1208.

Lagier-Tourenne C, Polymenidou M, Hutt KR, Vu AQ, Baughn M, Huelga SC, Clutario KM, Ling SC, Liang TY, Mazur C, *et al.* (2012). Divergent roles of ALS-linked proteins FUS/TLS and TDP-43 intersect in processing long pre-mRNAs. Nat Neurosci 15, 1488–1497.

Lin Y, Currie SL, Rosen MK (2017). Intrinsically disordered sequences enable modulation of protein phase separation through distributed tyrosine motifs. J Biol Chem 292, 19110–19120.

Liu LF, Desai SD, Li TK, Mao Y, Sun M, Sim SP (2000). Mechanism of action of camptothecin. Ann NY Acad Sci 922, 1–10.

Mastrocola AS, Kim SH, Trinh AT, Rodenkirch LA, Tibbetts RS (2013). The RNA-binding protein fused in sarcoma (FUS) functions downstream of poly(ADP-ribose) polymerase (PARP) in response to DNA damage. J Biol Chem 288, 24731–24741.

Mavragani IV, Nikitaki Z, Souli MP, Aziz A, Nowsheen S, Aziz K, Rogakou E, Georgakilas AG (2017). Complex DNA damage: a route to radiation-induced genomic instability and carcinogenesis. Cancers (Basel) 9, E91.

Monahan Z, Ryan VH, Janke AM, Burke KA, Rhoads SN, Zerze GH, O'Meally R, Dignon GL, Conicella AE, Zheng W, *et al.* (2017). Phosphorylation of the FUS low-complexity domain disrupts phase separation, aggregation, and toxicity. EMBO J 36, 2951–2967.

Montecucco A, Zanetta F, Biamonti G (2015). Molecular mechanisms of etoposide. EXCLI J 14, 95–108.

Murakami T, Qamar S, Lin JQ, Schierle GS, Rees E, Miyashita A, Costa AR, Dodd RB, Chan FT, Michel CH, *et al.* (2015). ALS/FTD mutation-induced

phase transition of FUS liquid droplets and reversible hydrogels into irreversible hydrogels impairs RNP granule function. Neuron 88, 678–690.
Murray DT, Kato M, Lin Y, Thurber KR, Hung I, McKnight SL, Tycko R (2017). Structure of FUS protein fibrils and its relevance to self-assembly and phase separation of low-complexity domains. Cell 171, 615–627.e16.
Neumann M, Rademakers R, Roeber S, Baker M, Kretzschmar HA, Mackenzie IR (2009). A new subtype of frontotemporal lobar degeneration with FUS pathology. Brain 132, 2922–2931.
Patel A, Lee HO, Jawerth L, Maharana S, Jahnel M, Hein MY, Stoynov S, Mahamid J, Saha S, Franzmann TM, *et al.* (2015). A liquid-to-solid phase transition of the ALS protein FUS accelerated by disease mutation. Cell 162, 1066–1077.
Povirk LF (1996). DNA damage and mutagenesis by radiomimetic DNA-cleaving agents: bleomycin, neocarzinostatin and other enediynes. Mutat Res 355, 71–89.
Rappsilber J, Friesen WJ, Paushkin S, Dreyfuss G, Mann M (2003). Detection of arginine dimethylated peptides by parallel precursor ion scanning mass spectrometry in positive ion mode. Anal Chem 75, 3107–3114.
Rastogi RP, Richa Kumar A, Tyagi MB, Sinha RP (2010). Molecular mechanisms of ultraviolet radiation-induced DNA damage and repair. J Nucleic Acids 2010, 592980.
Rogelj B, Easton LE, Bogu GK, Stanton LW, Rot G, Curk T, Zupan B, Sugimoto Y, Modic M, Haberman N, *et al.* (2012). Widespread binding of FUS along nascent RNA regulates alternative splicing in the brain. Sci Rep 2, 603.
Sama RR, Ward CL, Kaushansky LJ, Lemay N, Ishigaki S, Urano F, Bosco DA (2013). FUS/TLS assembles into stress granules and is a prosurvival factor during hyperosmolar stress. J Cell Physiol 228, 2222–2231.
Scaramuzzino C, Monaghan J, Milioto C, LansonNA Jr, Maltare A, Aggarwal T, Casci I, Fackelmayer FO, Pennuto M, Pandey UB (2013). Protein arginine methyltransferase 1 and 8 interact with FUS to modify its subcellular distribution and toxicity in vitro and in vivo. PLoS One 8, e61576.
Schindelin J, Arganda-Carreras I, Frise E, Kaynig V, Longair M, Pietzsch T, Preibisch S, Rueden C, Saalfeld S, Schmid B, *et al.* (2012). Fiji: an open-source platform for biological-image analysis. Nat Methods 9, 676–682.
Schwartz JC, Podell ER, Han SS, Berry JD, Eggan KC, Cech TR (2014). FUS is sequestered in nuclear aggregates in ALS patient fibroblasts. Mol Biol Cell 25, 2571–2578.
Sharma A, Lyashchenko AK, Lu L, Nasrabady SE, Elmaleh M, Mendelsohn M, Nemes A, Tapia JC, Mentis GZ, Shneider NA (2016). ALS-associated mutant FUS induces selective motor neuron degeneration through toxic gain of function. Nat Commun 7, 10465.
Shewmaker F, Wickner RB, Tycko R (2006). Amyloid of the prion domain of Sup35p has an in-register parallel beta-sheet structure. Proc Natl Acad Sci USA 103, 19754–19759.
Shrivastav M, De Haro LP, Nickoloff JA (2008). Regulation of DNA double-strand break repair pathway choice. Cell Res 18, 134–147.
Stepczynska A, Lauber K, Engels IH, Janssen O, Kabelitz D, Wesselborg S, Schulze-Osthoff K. (2001). Staurosporine and conventional anticancer drugs induce overlapping, yet distinct pathways of apoptosis and caspase activation. Oncogene 20, 1193–1202.
Sun S, Ling SC, Qiu J, Albuquerque CP, Zhou Y, Tokunaga S, Li H, Qiu H, Bui A, Yeo GW, *et al.* (2015). ALS-causative mutations in FUS/TLS confer gain and loss of function by altered association with SMN and U1-snRNP. Nat Commun 6, 6171.
Tan AY, Riley TR, Coady T, Bussemaker HJ, Manley JL (2012). TLS/FUS (translocated in liposarcoma/fused in sarcoma) regulates target gene transcription via single-stranded DNA response elements. Proc Natl Acad Sci USA 109, 6030–6035.
Tradewell ML, Yu Z, Tibshirani M, Boulanger MC, Durham HD, Richard S (2011). Arginine methylation by PRMT1 regulates nuclear-cytoplasmic localization and toxicity of FUS/TLS harbouring ALS-linked mutations. Hum Mol Genet 21, 136–149.
Vance C, Rogelj B, Hortobagyi T, De Vos KJ, Nishimura AL, Sreedharan J, Hu X, Smith B, Ruddy D, Wright P, *et al.* (2009). Mutations in FUS, an RNA processing protein, cause familial amyotrophic lateral sclerosis type 6. Science 323, 1208–1211.
Wang WY, Pan L, Su SC, Quinn EJ, Sasaki M, Jimenez JC, Mackenzie IR, Huang EJ, Tsai LH (2013). Interaction of FUS and HDAC1 regulates DNA damage response and repair in neurons. Nat Neurosci 16, 1383–1391.
Xu Y, Her C (2015). Inhibition of topoisomerase (DNA) I (TOP1): DNA damage repair and anticancer therapy. Biomolecules 5, 1652–1670.
Yang F, Teves SS, Kemp CJ, Henikoff S (2014a). Doxorubicin, DNA torsion, and chromatin dynamics. Biochim Biophys Acta 1845, 84–89.
Yang L, Gal J, Chen J, Zhu H (2014b). Self-assembled FUS binds active chromatin and regulates gene transcription. Proc Natl Acad Sci USA 111, 17809–17814.
Yasuda K, Zhang H, Loiselle D, Haystead T, Macara IG, Mili S (2013). The RNA-binding protein Fus directs translation of localized mRNAs in APC-RNP granules. J Cell Biol 203, 737–746.
Zein N, Sinha AM, McGahren WJ, Ellestad GA (1988). Calicheamicin gamma 1I: an antitumor antibiotic that cleaves double-stranded DNA site specifically. Science 240, 1198–1201.